ASE narrow-band noise pulsing in erbium-doped fiber amplifier and its effect on self-phase modulation

Pablo Muniz-Cánovas,[1] **Yuri O. Barmenkov,**[1,2,*] **Alexander V. Kir'yanov,**[1,3] **Jose L. Cruz,**[2] **and Miguel V. Andrés**[2]

[1]*Centro de Investigaciones en Optica, Loma del Bosque 115, Col. Lomas del Campestre, Leon 37150, Mexico*
[2]*Departamento de Fisica Aplicada, Instituto de Ciencia de Materiales, Universidad de Valencia, 46100 Valencia, Spain*
[3]*National University of Science and Technology "MISIS", Moscow 119049, Russian Federation*
[*]*yuri@cio.mx*

Abstract: In this paper, we report a study of the features of polarized and unpolarized narrow-band amplified spontaneous emission (ASE) in a low-doped erbium fiber at 976-nm pumping. We demonstrate that ASE noise can be treated as a train of Gaussian-like pulses with random magnitudes, widths, and inter-pulse intervals. ASE noise can also provide a statistical analysis of these three parameters. We also present the data that reveal ASE noise's role in optical spectrum broadening through self-phase modulation of light propagating in a communication fiber. In particular, the data show that the ASE noise derivative defines the broadening's spectral shape.

1. Introduction

Amplified spontaneous emission (ASE) based light sources are characterized by the broad optical spectrum and high temporal stability, given the absence of relaxation oscillations and interference effects. Such kind of light sources are successful in many applications, including high-precision fiber-optic gyroscopes [1,2], low-coherence interferometry [3], optical coherence tomography [4,5], *etc*. Recently, it was demonstrated that nanosecond ASE pulses produced by actively Q-switched fiber lasers may provide an effective pump for supercontinuum generation [6–9]. ASE sources may also serve as seed for CW amplifying to a multi-hundred watts level with inherently suppressed SBS because of the broad ASE spectrum [10–12]. On the other hand, in fiber amplifiers used in fiber-optic links, ASE noise is naturally added to amplified signal, thus deteriorating the signal-to-noise ratio [13–16].

ASE noise is described [17,18] by M-fold degenerate Bose-Einstein distribution, with M being the number of independent states (modes) of ASE, defined by the ratio of its optical spectrum width (B_{opt}) to photodetector electric bandwidth (B_{el}) and polarization degeneracy (s); generally, M is a real positive number, equal to or higher than 1. The basic properties of ASE noise statistics are known; nonetheless, knowledge of fine details of ASE noise pulsing is important for deeper understanding the nonlinear effects in optical fibers, supercontinuum generation using ASE signal as a pump, physics of frequency-shifted fiber lasers, rogue waves phenomenon, and so on.

In this paper, we report the experimental results on ASE pulsing, inherent to an erbium-doped fiber amplifier (EDFA) at the conditions of spectral filtering by fiber Bragg gratings (FBGs). Herewith, we assess the case when the optical filtering is much narrower than the electrical one ($B_{opt}/B_{el} << 1$), which gives rise to single ASE mode for polarized ($s = 1$) light and two ASE modes for unpolarized ($s = 2$) light. We show that noise pulses of which ASE signal is composed are Gaussian-like, with magnitudes, widths, and sequencing intervals described by specially parameterized distributions. Also, we demonstrate that the distribution

of ASE timing derivatives defines the shape of optical spectrum broadening via self-phase modulation: namely, it gets symmetric triangular-like form when plotted in semi-logarithmic scale. The data on spectral broadening of ASE signal passed through a long communication fiber confirms the claim.

2. Experimental setup

The experimental setup is shown in Fig. 1. It comprises a seed ASE source based on erbium-doped fiber EDF1 and a fiber amplifier based on EDF2. The EDF used in both stages was a standard low-doped M5-980-125 fiber with small-signal gain of ~6.5 dB/m at 1530 nm. These EDFs were pumped by commercial 976-nm diode lasers through fused 976/1550 nm wavelength division multiplexers (WDMs). Lengths of EDF1 and EDF2 were ~6 m each; this provided relatively high ASE power and, at the same time, prevented parasitic CW lasing (otherwise, if the active fiber is too long, spurious lasing may arise at 1530 nm on weak reflections from the fiber components [20]). For the same purpose, *viz*. for avoiding parasitic lasing, a long-period grating (LPG) with attenuation peak at 1530 nm was utilized in the scheme. Circulators (C1 and C2) served for preventing feedbacks between the seed ASE source, the fiber amplifier, and the output fiber patch-cord with PC/APC termination. A fiber polarizer (POL) was placed at the setup output for exploring the properties of polarized ASE; otherwise, i.e. when unpolarized output was under study, it was removed.
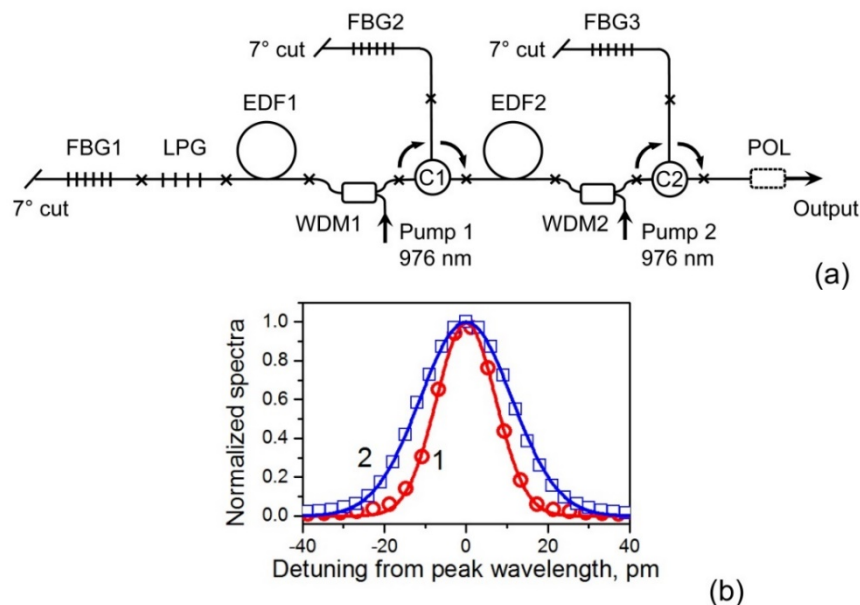

Fig. 1. (a) Experimental arrangement of ASE source; crosses indicate fiber splices. (b) Normalized spectra of OSA response to narrow-band laser line (line 1) and ESA spectrum (line b). Lines are Gaussian fits.

To select the operation wavelength and the optical bandwidth of the ASE source, a set of three home-made fiber Bragg gratings (FBGs 1 to 3) centered at 1544.6 nm was used. FBG1 was broadband (~600 pm at half of reflection maximum (FWHM)) while FBG2 and FBG3 were much narrower (45 pm and 27 pm FWHM, respectively). The ASE spectrum measured at the output port of circulator C2 was Gaussian (26.4 pm FWHM; see curve 1 in Fig. 1(b)). Since the response of the optical spectrum analyzer (OSA) to the narrow-line (130 kHz) laser signal was as well Gaussian-like (17.2 pm FWHM; see curve 2 in Fig. 1(b)), we decomposed

the spectral functions of ASE and OSA for estimating a real ASE bandwidth, found to be 20 pm (or 2.5 GHz).

ASE signals were detected by a 25-GHz InGaAs Schottky photodetector (*Newport*, model 1414) connected to a 16-GHz real-time oscilloscope (*Tektronix*, model DPO71604C); overall RF band of this set of equipment extends from DC to factual 15.5 GHz (measured at a 3-dB level). In the experiments, output ASE power was set to ~2 mW, to ensure the photodetector operation well below saturation.

3. Experimental results and discussion

First, we checked whether the statistics of ASE signals are properly described by the *M*-fold degenerate Bose-Einstein distributions. We measured histograms for both polarized and unpolarized ASE; then, these were fitted by curves, simulated using the following formula for Bose-Einstein distribution [17,18]:

$$P\left(n,\overline{n},M\right) = \frac{(n+M-1)!}{n!(M-1)!}\frac{\left(\overline{n}\right)^{n}}{\left(1+\overline{n}\right)^{n+M}} \tag{1}$$

where $P(n,\overline{n},M)$ is the probability of counting n photons by photodetector during averaged time $T = 1/B_{el}$, $\overline{n}$ is the mean photon count within the same time interval, and M is the number of independent ASE states (modes), defined, for the Gaussian optical spectrum, as [17,18]:

$$M = s\frac{\pi\left(B_{opt}/B_{el}\right)^{2}}{\pi\left(B_{opt}/B_{el}\right)\mathrm{erf}\left[\sqrt{\pi}\left(B_{opt}/B_{el}\right)\right]-\left[1-\exp\left(-\pi\left(B_{opt}/B_{el}\right)^{2}\right)\right]} \tag{2}$$

At our experimental conditions, the ratio B_{opt}/B_{el} is 0.16; thus, $M \approx 1.13$ for polarized ASE and ≈ 2.27 for unpolarized one. Note that, for $M = 1$ and large $\overline{n}$, formula (1) can be reduced to the exponential decay function:

$$P\left(n,\overline{n},M\right) \approx \frac{1}{\overline{n}}\exp\left(-\frac{n}{\overline{n}}\right) \propto \exp\left(-\frac{P}{P_{0}}\right) \tag{3}$$

where P is ASE power and P_0 is its mean value. ASE distribution approximated by the exponential probability density function (PDF) (see formula (3)) is Gaussian for the field, as is assumed, for instance, in wave turbulence theory for the weakly nonlinear regime [21,22].

In Fig. 2, we present two examples of the experimental histograms of ASE noise, obtained for (a) polarized ($s = 1$) and (b) unpolarized ($s = 2$) lights and their fits. In the two panels, the horizontal axes are normalized to the mean photon number (proportional to the mean voltage of photodetector) and the vertical axes are recalculated into probabilities. In both cases, the fitting curves obtained using Eq. (1) with "optimal" *M*-values (at best fitting) are demonstrated by the green lines. For comparison, we add the histograms, simulated for the "ideal" case when $M = 1$ (polarized light) and $M = 2$ (unpolarized light), shown by the red lines. The fitting curves were simulated using the mean photon number $\overline{n} = 1.1 \times 10^{6}$, corresponding to the experimental conditions ($P_0 = 2$ mW and $B_{opt} = 2.5$ GHz).
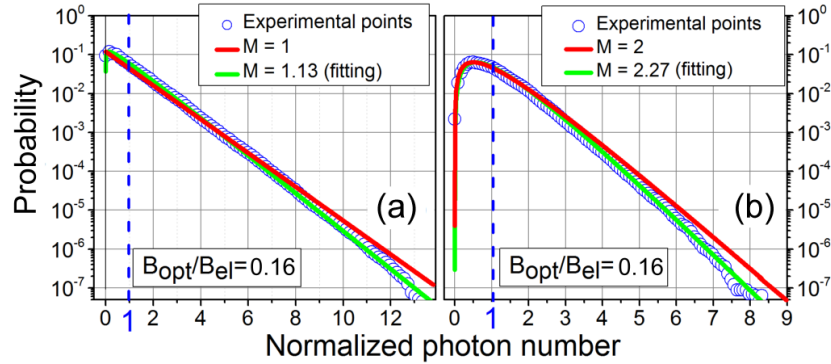
Fig. 2. Histograms of probability (PDF) of the normalized photon number (ASE noise voltage). Histograms obtained for polarized ($s = 1$) and unpolarized ($s = 2$) ASE are shown in the left and right panel, respectively. Circles are experimental points, green lines are the best fits, and red lines are simulated probabilities for the ideal cases: $M = 1$ at $s = 1$ and $M = 2$ at $s = 2$

As seen from Fig. 2, the experimental histograms are suitably described by the M-fold degenerate Bose-Einstein distributions, where M-values stand for the best fits using formula (2). This reveals that ASE light in our case is a classical thermal source. It is also seen from Fig. 2 that, even for the small ratio B_{opt}/B_{el} (<<1), the mode number M is always above 1 and 2, for polarized and unpolarized ASE, respectively, given that the absolute slope values for the red curves are always lower than those for the fitting lines.

Figure 3 presents the two examples of randomly chosen short sections of the oscilloscope traces selected from the long ones, as captured for (a) polarized and (b) unpolarized ASE. These were obtained at the same conditions at which the histograms shown in Fig. 2 were recorded (i.e. for $M = 1.13$ and $M = 2.27$, respectively). In Fig. 2, circles are the experimental points, triangles are the peaks' magnitudes, and the solid lines are the Gaussian fits of noise peaks. As seen from Fig. 3, ASE noise presents trains of noise pulses with randomly varying magnitudes, widths, and sequencing intervals, where each pulse may be fitted by the Gaussian function, permitting determination of pulse width and location in the train.
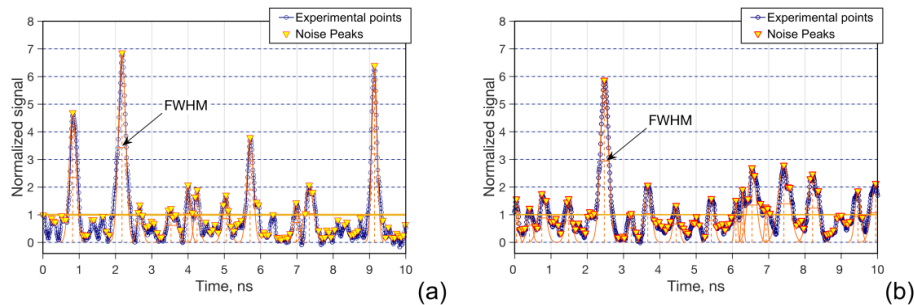

Fig. 3. ASE noise as train of Gaussian-like pulses (circles) measured for (a) polarized and (b) unpolarized ASE normalized to the mean values of photodetector signal. Vertical dash lines indicate centers of Gaussian fits; here, the pulses with magnitude less than the mean are not fitted. The intervals between adjacent points are 10 ps.

Figure 4 shows the histograms of probability of ASE noise pulse magnitudes, obtained from the long oscilloscope traces (31.25 mega-samples, the oscilloscope's limit), for both polarized and unpolarized ASE; the stars stand for the experimental probabilities of the noise peak magnitudes, normalized to the mean value of the ASE signal. As seen, these two dependences are located above the theoretical ones simulated for the ideal case described by the Bose-Einstein distribution with $M = 1$ and $M = 2$ (dash lines), for polarized and unpolarized light, respectively.
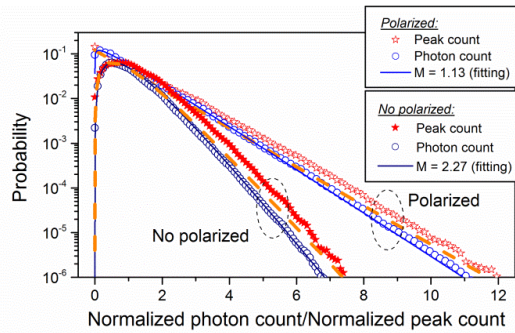
Fig. 4. Histograms measured for magnitudes of ASE peaks (stars) and photon counts (circles). Both dependences of photon count and ASE peaks are normalized to the mean photon count. Lines are theoretical dependencies.

For comparison, probabilities of photon counts (also shown in Fig. 2), together with the best fits, are provided in Fig. 4, too (see solid lines). As seen, the histograms of the peak counts are broader than those for the photon counts. This seems to stem from the fact that photon counts relate to all experimental points, not only to points at tops of ASE pulses. Note that occasional excessive noise peaks with magnitudes much greater than the mean power may be treated as rogue waves or their seeds [7,23–25].

Another important issue regarding ASE pulsing is dispersion of the intervals between pulses belonging to different ranges of magnitudes (P); refer to Fig. 3. Such ranges were identified in the following manner: (*i*) below the mean photon count (m), (*ii*) from the mean to two means, (*iii*) from two to three means *etc*., but with a limit being $P = 9m$ to $10m$ (at higher peak magnitudes, the peak counts are too small to be proceed for a statistical analysis).

Figure 5(a) demonstrates two examples of semi-logarithmic plots of histograms for intervals between polarized ASE pulses, belonging to two different ranges of magnitudes, as specified in panels (a1) and (a2). The histograms are fit with a high confidence by linear dependences, which reveals exponential decay of the peak count *vs*. interval between pulses. The vertical dash lines in both panels correspond to the intervals between pulses at which the peak count drops by half and the horizontal dash lines indicate −3 dB levels respectively to the peak count at ~200-ps interval. Unpolarized ASE pulses obey a similar trend (not shown).

The fits obtained for all processed peaks' magnitudes were used for making-up Fig. 5(b), showing 3D dependence of the fits for peak counts, normalized to maximum (color scaling), in function of normalized magnitude and inter-pulse interval (or sequencing time).
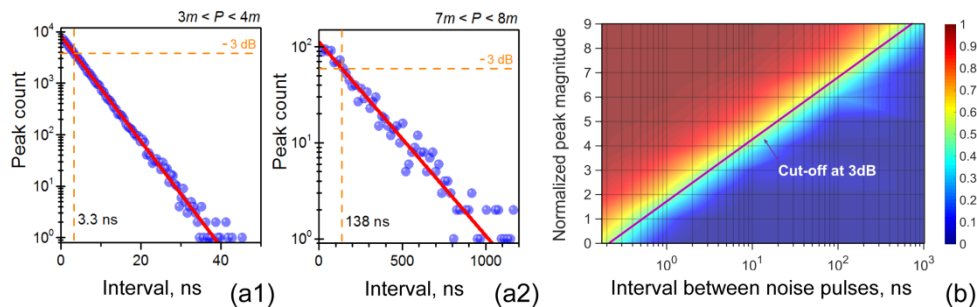

Fig. 5. (a) Examples of histograms for intervals between ASE pulses, belonging to the ranges of the normalized peak magnitudes limited to (a1) $3m$ to $4m$ and (a2) $7m$ to $8m$. ASE is polarized. Symbols are experimental data and lines are exponential fits. (b) Peak count normalized to its maximum (color scale) in function of normalized peak magnitude and interval between peaks of the same ranges of magnitude.

It is seen that probability of shorter intervals between adjacent peaks of the same range of magnitudes is higher, while probability of longer intervals decays exponentially with increasing peaks amplitude. The higher magnitude of ASE peaks, the decay is slower. Note that in Fig. 5 the peaks' separation is fixed to 175 ps, the minimal value (corresponding to the width of a transform-limited Gaussian pulse with optical spectrum of 20 pm, or 2.5 GHz in frequency domain) to be resolved [26]. Note that the "cut-off" value of the interval between peaks, Δt, measured at −3 dB below the maximal peak count (for short time intervals, refer to Figs. 5(a1) and 5(a2)), also increases exponentially with increasing P: see the diagonal line in Fig. 5(b). This line divides the graph surface in two triangular subareas with maximal (red color) and minimal (blue color) values of the normalized peak count, with a narrow transitional area of width around the magnitude of intervals between consecutive pulses.
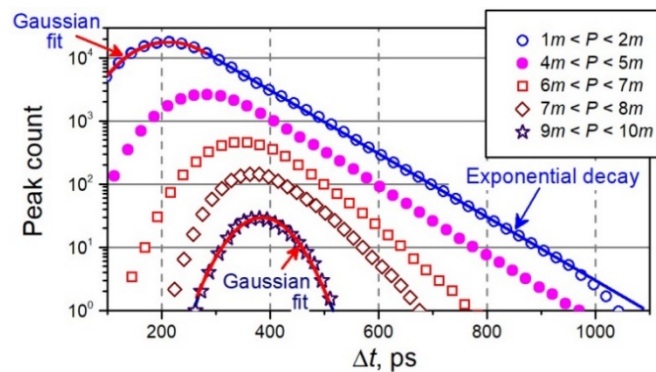

Fig. 6. Examples of histograms of ASE pulses' width, obtained for different normalized peak magnitudes P. Symbols indicate experimental points and lines are some examples of fits. The blue line is exponential fit whereas the red lines are Gaussian ones.

In Fig. 6, are resumed the histograms of FWHM width (Δt) of polarized ASE, parameterized for different P-ranges. As seen, both the shapes of the histograms and the most probabilistic widths depend on pulse magnitude. Furthermore, all the histograms obtained for $P < 5m$ are seen to be shaped very similarly (compare the two upper curves); however, for higher P, the histograms become more symmetrical (see the lower curves) and narrow.

Interestingly, for small peak powers ($P < 5m$), the left slopes of the histograms look Gaussian-like and their right slopes have exponential form, whereas for the highest peak power, the histogram (lowest in Fig. 6) is fit as the whole by the Gaussian function. The relative width (FWHM divided by the most probable value) of the upper histogram, obtained for $1m < P < 2m$, is 0.86, whilst that of the lowest one, obtained for $9m < P < 10m$, is 0.3 (~3 times less). Thus, dispersion of ASE noise pulses notably decreases with increasing peak power.

Figure 7(a) demonstrates the histograms of the normalized derivative for large train of ASE pulses (short sections are shown in Fig. 3), found as $\Delta V/\Delta t/V_{mean}$, for polarized (red dots) and unpolarized (blue rectangles) ASE, where ΔV is the voltage difference between two adjacent experimental points, $\Delta t = 10$ ps is the interval between them, and V_{mean} is the mean voltage. As seen, the derivatives of ASE signals in both cases are triangular in semi-logarithmic scale (which correspond to exponential decays in linear scale) and symmetric with respect to the vertical dash line (at least within ~60-dB range of magnitude); width of the histogram for polarized ASE is ~2 times greater than that for unpolarized ASE. The triangular shape of the derivative itself results from the linear distribution of magnitudes of ASE peaks when it is presented in semi-logarithmic scale (Fig. 4). In turn, the difference in the histograms' widths is explained by the fact that the histograms themselves are broader for polarized light than for unpolarized light (refer to Fig. 2); this means that noise pulses arising

with the same probability are more powerful and their derivatives are also greater in the first (polarized light) case.
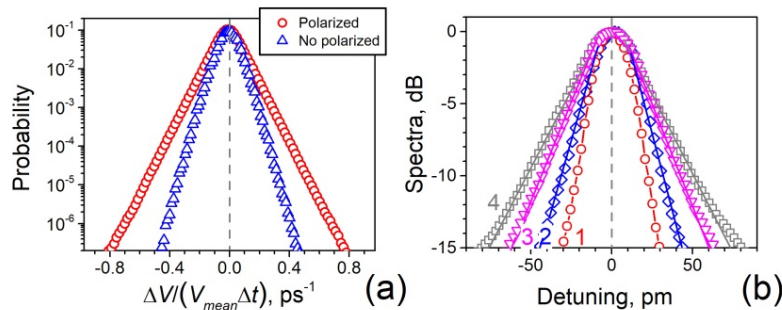

Fig. 7. (a) Histogram of normalized derivative of polarized (circles) and unpolarized (triangles) ASE noise. (b) Normalized spectrum of ASE signal on input of long communication fiber (line 1) and broadened normalized spectra measured at the fiber output (lines 2 to 4); all spectra are normalized to maxima. Symbols are experimental points and solid lines are fits. In panel (a) detuning is given respectively to ASE peak wavelength (1544.6 nm).

Figure 7(b) demonstrates the effect of ASE spectrum broadening after propagating 20 km of standard communication fiber (SMF-28); ASE polarization at the fiber entrance was random. In the experiment, a scalable optical amplifier of the "seed" ASE source (discussed above) was used, permitting to scale ASE power up to 82 mW while keeping unchanged the ASE spectral width. If one takes 100 ps as the lowest pulse-width limit, the nonlinear length of the fiber is ~10 km or less; hence, the nonlinear effects appear to be much stronger than the broadening of ASE pulses because the fiber's dispersion length is ~500 km.

Curve 1 in Fig. 7(b) shows the spectrum of ASE signal at the fiber input; its shape is clearly Gaussian with the same width as that shown in Fig. 1(b). Curves 2 to 4 show the ASE spectra at the fiber output for input powers of 30, 52, and 82 mW, respectively; steady and symmetrical broadening of the spectra with increasing ASE power is evident from the spectra' comparison. The broadened spectra, likewise the histograms of ASE derivatives (refer to Fig. 7(a)), are characterized by almost triangular profiles when plotted in semi-logarithmic scale. Slight discrepancy from the triangularity, observed below −13 dB for maximal ASE power, arises owing to modulation instability. For example, for maximal ASE power (82 mW), an estimated nonlinear phase shift ϕ_{NL} due to SPM mainly matches the range from zero to 10 rad (at P varied from $0m$ to $10m$) and even to larger values for extremely rare events; at $P = P_{mean}$, $\phi_{NL} = 1$ rad.

Note that the inherent to SPM ASE spectral broadening in optical fiber and its dispersion were recently modeled [19] in assumption that ASE as pump for SCG is harmonically modulated signal with some average frequency and magnitude. The found above laws may shed more light on the physics behind the phenomenon.

4. Conclusion

In this paper, we presented the data on noise properties of amplified spontaneous emission (ASE), outcoming a standard low-doped erbium fiber. ASE was optically filtered using a set of home-made fiber Bragg gratings (FBGs). The obtained ASE spectra were nearly Gaussian with FWHM of 20 pm (2.5 GHz), i.e. much narrower than the combined RF band of the set of experimentally used photodetector (25 GHz) and oscilloscope (16 GHz). We also discussed the effect of narrow-band ASE of moderate (~100 mW) power upon character of spectral broadening at propagating along a communication fiber.

First, we proved that ASE photon statistics is of thermal type as it is described by M-fold degenerate Bose-Einstein distribution with M depending on optical spectrum width and number of polarization states. Also, we found that, for polarized ASE, the degeneracy factor

(mode number) M is always above unity and, hence, the photon statistics never obeys an exponential law.

Second, we considered some specific features, relevant to narrow-band ASE noise. It was shown that it may be represented by train of Gaussian-like pulses with randomly distributed magnitudes, widths, and sequencing intervals. The probability distributions of pulse magnitudes slightly deviate from the "ideal" cases ($M = 1$ and $M = 2$ for polarized and unpolarized light, respectively) but their slopes are kept nearly the same. Besides, it was demonstrated that count of intervals between ASE pulses of the same magnitude fades exponentially with increasing the interval between pulses: the bigger pulse magnitude, the slower decay is.

Third, we characterized in detail the distributions of width of ASE pulses in function of their magnitudes. For pulse magnitudes below five-means of ASE power, the histograms are strongly asymmetric and broad and their left and right slopes are described in time domain by the Gaussian and exponential functions, respectively. At increasing pulse magnitudes, the histograms become narrower and more symmetric. Besides, for pulses with higher magnitude (above nine-means of ASE power), the histograms match Gaussian distributions. This signifies that more powerful ASE pulses are more stable in width than less powerful ones. Importantly, the most probabilistic pulse-width increases with pulse magnitude (from ~200 ps for the smallest pulses to ~400 ps for the highest ones).

Finally, we examined the influence of ASE pulsing upon broadening of the optical spectrum at propagating along a communication fiber and demonstrated that the shape of broadening at the fiber's output is defined by that of ASE noise derivative (triangular at semi-logarithmic scaling), characteristic to SPM at weak nonlinearity.

Funding

References

1. D. Guillaumond and J. P. Meunier, "Comparison of two flattening techniques on a double-pass erbium-doped superfluorescent fiber source for fiber-optic gyroscope," IEEE J. Sel. Top. Quantum Electron. **7**(1), 17–21 (2001).
2. A. B. Petrov, R. Gumenyuk, M. S. Alimbekov, P. E. Zhelezov, N. E. Kikilich, A. S. Aleynik, I. K. Meshkovsky, K. M. Golant, Y. K. Chamorovskii, M. Odnoblyudov, and V. Filippov, "Broadband superluminescent erbium source with multiwave pumping," Opt. Commun. **413**, 304–309 (2018).
3. P. F. Wysocki, M. J. F. Digonnet, B. Y. Kim, and H. J. Shaw, "Characteristics of erbium-doped superfluorescent fiber sources for interferometric sensor applications," J. Lightwave Technol. **12**(3), 550–567 (1994).
4. S. G. Proskurin, "Raster scanning and averaging for reducing the influence of speckles in optical coherence tomography," Quantum Electron. **42**(6), 495–499 (2012).
5. Y. Rao, N. P. Sarwade, and R. Makkar, "Modeling and Simulation of Optical Coherence Tomography on Virtual OCT," Procedia Comput. Sci. **45**, 644–650 (2015).
6. A. Jin, H. Zhou, X. Zhou, J. Hou, and Z. Jiang, "High-power ultraflat near-infrared supercontinuum generation pumped by a continuous amplified spontaneous emission source," Photon. J. **24**(3), 0900710 (2018).
7. A. Mussot, A. Kudlinski, M. Kolobov, E. Louvergneaux, M. Douay, and M. Taki, "Observation of extreme temporal events in CW-pumped supercontinuum," Opt. Express **17**(19), 17010–17015 (2009).
8. J. A. Minguela-Gallardo, Y. O. Barmenkov, A. V. Kir'yanov, and G. Beltrán-Pérez, "Photon statistics of actively Q-switched erbium-doped fiber laser," J. Opt. Soc. Am. B **34**(7), 1407–1417 (2017).
9. P. Harshavardhan Reddy, A. V. Kir'yanov, A. Dhar, S. Das, D. Dutta, M. Pal, Y. O. Barmenkov, J. A. Minguela-Gallardo, S. K. Bhadra, and M. C. Paul, "Fabrication of ultra-high numerical aperture GeO$_2$-doped fiber and its use for broadband supercontinuum generation," Appl. Opt. **56**(33), 9315–9324 (2017).
10. P. Wang and W. A. Clarkson, "High-power, single-mode, linearly polarized, ytterbium-doped fiber superfluorescent source," Opt. Lett. **32**(17), 2605–2607 (2007).

11. O. Schmidt, M. Rekas, C. Wirth, J. Rothhardt, S. Rhein, A. Kliner, M. Strecker, T. Schreiber, J. Limpert, R. Eberhardt, and A. Tünnermann, "High power narrow-band fiber-based ASE source," Opt. Express **19**(5), 4421–4427 (2011).

12. J. Xu, P. Zhou, W. Liu, J. Leng, H. Xiao, P. Ma, J. Wu, H. Zhang, J. Chen, and Z. Liu, "Exploration in performance scaling and new application avenues of superfluorescent fiber source," IEEE J. Sel. Top. Quantum Electron. **24**(3), 1 (2018).

13. T. Li and M. C. Teich, "Bit-error rate for a lightwave communication system incorporating an erbium-doped fibre amplifier," Electron. Lett. **27**(7), 598 (1991).

14. P. Diament and M. C. Teich, "Evolution of the statistical properties of photons passed through a travel-wave laser amplifier," IEEE J. Quantum Electron. **28**(5), 1325 (1992).

15. T. Li and M. C. Teich, "Photon point process for traveling-wave laser-amplifiers," IEEE J. Quantum Electron. **29**(9), 2568–2578 (1993).

16. A. Mecozzi, "Quantum and semiclassical theory of noise in optical transmission lines employing in-line erbium amplifiers," J. Opt. Soc. Am. B **17**(4), 607–617 (2000).

17. J. W. Goodman, *Statistical Optics*, New York (Wiley, 2000).

18. S. M. Pietralunga, P. Martelli, and M. Martinelli, "Photon statistics of amplified spontaneous emission in a dense wavelength-division multiplexing regime," Opt. Lett. **28**(3), 152–154 (2003).

19. Q. Li, H. Zhang, X. Shen, H. Hao, and M. Gong, "Phenomenological model for spectral broadening of incoherent light in fibers via self-phase modulation and dispersion," J. Opt. **18**(11), 11503 (2016).

20. Y. O. Barmenkov, A. V. Kir'yanov, J. L. Cruz, and M. V. Andrés, "Dual-kind Q-switching of erbium fiber laser," Appl. Phys. Lett. **104**(9), 091124 (2014).

21. A. Picozzi, J. Garnier, T. Hansson, P. Suret, S. Randoux, G. Millot, and D. N. Christodoulides, "Optical wave turbulence: Towards a unified nonequilibrium thermodynamic formulation of statistical nonlinear optics," Phys. Rep. **542**(1), 1–132 (2014).

22. G. Xu, J. Garnier, A. Mussot, S. Trillo, D. Churkin, N. Tarasov, S. Turitsyn, and A. Picozzi, "Weak Langmuir optical turbulence in a fiber cavity," Phys. Rev. A (Coll. Park) **94**(1), 013823 (2016).

23. J. He, S. Xu, and K. Porsezian, "New Types of Rogue Wave in an Erbium-Doped Fibre System," J. Phys. Soc. Jpn. **81**(3), 033002 (2012).

24. S. Toenger, T. Godin, C. Billet, F. Dias, M. Erkintalo, G. Genty, and J. M. Dudley, "Emergent rogue wave structures and statistics in spontaneous modulation instability," Sci. Rep. **5**(1), 10380 (2015).

25. N. Akhmediev, B. Kibler, F. Baronio, M. Belić, W. Zhong, Y. Zhang, W. Chang, J. M. Soto-Crespo, P. Vouzas, P. Grelu, C. Lecaplain, K. Hammani, S. Rica, A. Picozzi, M. Tlidi, K. Panajotov, A. Mussot, A. Bendahmane, P. Szriftgiser, G. Genty, J. Dudley, A. Kudlinski, A. Demircan, U. Morgner, S. Amiraranashvili, C. Bree, G. Steinmeyer, C. Masoller, N. G. R. Broderick, A. F. J. Runge, M. Erkintalo, S. Residori, U. Bortolozzo, F. T. Arecchi, S. Wabnitz, C. G. Tiofack, S. Coulibaly, and M. Taki, "Roadmap on optical rogue waves and extreme events," J. Opt. **18**(6), 063001 (2016).

26. W. R. Leo, *Techniques for Nuclear and Particle Physics Experiments: A How-to Approach*, 2nd ed., Berlin, Germany (Springer-Verlag, 1994), chapter 5.3.